Nanomanipulation of Ligand Nanogeometry Modulates Integrin/Clathrin-Mediated Adhesion and Endocytosis of Stem Cells

Bohan Yin[†], *Qin Zhang*[†], *Jiaxiang Yan*[†], *Yingying Huang*[†], *Chuanqi Li*[†], *Jiareng Chen*[†], *Chunyi Wen*[†], *Siu Hong Dexter Wong*[†,§,*], *Mo Yang*[†,§,*]

[†]Department of Biomedical Engineering, The Hong Kong Polytechnic University, Kowloon, Hong Kong 999077, China

[§]Research Institute for Sports Science and Technology, The Hong Kong Polytechnic University, Kowloon, Hong Kong 999077, China

*Corresponding author:

Siu Hong Dexter Wong: shongwong@polyu.edu.hk

Mo Yang: mo.yang@polyu.edu.hk

KEYWORDS

Nanosubstrate engineering, ligand nanogeometry, cell–substrate interaction, endocytosis, stem cell differentiation

ABSTRACT

Nanosubstrate engineering is a biomechanical approach for modulating stem cell differentiation in tissue engineering. However, it remains unexplored to study the effect of clathrin-mediated processes on manipulating this behavior. Herein, we develop integrin-binding nanosubstrates at confined nanogeometries that regulate clathrin-mediated adhesion- or endocytosis-active signaling pathways for modulating stem fates. Isotropically presenting ligands in nanoscale enhances the expression of clathrin in cells, thereby facilitating uptake of dexamethasone-loaded nanoparticles (NPs) to boost osteogenesis of stem cells. In contrast, anisotropic ligand nanogeometry suppresses this clathrin-mediated NP entry by strengthening the association between clathrin and adhesion spots to reinforce mechanotransduced signaling, which can be abrogated by pharmacological inhibition of clathrin. Meanwhile, inhibiting focal adhesion formation hinders cell spreading and enables higher endocytosis efficiency. Our findings reveal the crucial roles of clathrin in both endocytosis and mechanotransduction of stem cells and provide the parameter of ligand nanogeometry for the rational design of biomaterials for tissue engineering.

Human mesenchymal stem cells (hMSCs) are a great potential source for regenerating damaged/injured tissue due to their self-renewal capability and multilineage differentiation potency.[1] Therefore, effectively guiding hMSCs toward specific lineage is of utmost importance in the field of tissue engineering.[2] In the past decades, the methods for manipulating hMSC differentiation (e.g., osteogenic differentiation) have been intensively investigated. Nanomaterial has emerged as an effective tool to enter stem cells owing to their small size and regulate stem cell differentiation via particular signaling pathways.[3] For instance, nanomaterials serve as nanocarriers with high loading capacity to deliver the potent inducer of osteogenesis [e.g., dexamethasone (Dex)] to augment osteogenic capability of stem cells.[1,4,5] Generally, clathrin-mediated endocytosis (CME) is the major pathway for nanoparticles (NPs) to enter the cells, with the formation of clathrin-coated pits and recruitment of related adaptor proteins [e.g., adaptor protein 2 (AP2)] on the cell membrane to form intracellular vesicle for delivering cargoes.[6,7] Therefore, recent studies exploited substrate engineering, such as optimizing its surface roughness,[8] topography,[9–11] or stiffness,[12,13] to promote the expression of CME-associated proteins for intracellular delivery of NPs.

Besides mediating cellular uptake of NPs, clathrin also involves in integrin-associated adhesion structures independently of its role in endocytosis.[14,15] Previous studies showed that the effective engagement between integrins and ligands recruited clathrin via AP2 to regulate the associated signalings.[16] Critically, this activation can be subject to biophysical cues of the microenvironment. For example, large and flat clathrin-coated plaques are formed on the stiff substrate to upregulate ERK activation, which is abrogated on the soft substrate.[17,18] It is known that Arg-Gly-Asp (RGD), a bioactive ligand of extracellular matrix (ECM), can specifically activate integrin β3 for cell adhesion.[16] Sheetz et al. reported that cells cultured on a substrate with mobile RGD exhibited

enhanced integrin-based CME activity, while this process was suppressed in cells on the fixed RGD substrate with mature focal adhesion (FA) formation.[16] These studies suggest that the key roles of integrin/clathrin can be interchanged in response to various conditions of ligand presentations. Material surfaces with nano/micro features can modulate CME functions of cells.[19–22] Hence, it is highly possible that the subcellular level interactions between cell receptors and bioactive molecules can regulate CME activity. Therefore, controlling the nanogeometric display of specific ligands may potentially unravel how integrin and clathrin are recruited to "turn on" the endocytosis- or adhesion-active state.

Integrin-ligand binding occurs in nanoscale. Thus, precisely controlling the nanoscale display of ligands is critical to orthogonally investigate cell-material interactions.[23–26] In particular, ligand clustering and nanospacing controlled by nanostructures are pivotal for activating integrin and the associated signaling.[27–30] We also demonstrated that manipulating local clustering,[31] tether mobility,[32] or physical caging[33] of RGD-displaying nanoparticles regulated cell adhesion and fates. A recent study revealed that MC3T3 preosteoblasts cultured on nanogrooved substrates showed enhanced cytoskeletal structures and mature FA but exhibited poor endocytic uptake of cell penetrating peptides compared to those on flat control.[34] Nevertheless, how these nanofeatures directly regulate integrin/clathrin activation remains elusive. It is conducive to controlling the nanogeometric presentation but decoupling the other effects of the ligand arrangement in the nanoscale (e.g., ligand density) on cell adhesion/endocytosis.

Herein, we engineer cell seeding nanosubstrates by coating gold nanospheres (AuNPs) with an aspect ratio (AR) of 1 (AR1-S) or gold nanorods (AuNRs) with an AR of 4 (AR4-S), respectively. The random-oriented coating of AR4 ensures the anisotropy presentation of RGD peptides at nanoscale instead of micro/macroscale to cell receptors.[35] The choice of these two aspect ratios

(AR1 and AR4) was based on the critical threshold of the effective development of traction forces in cells that were cultured on substrates with AuNR of larger AR (≥ 4).[35] We aim to adopt the well-established anisotropic AuNRs to study the interplay among 1) nanogeometric ligand presentation, 2) integrin/clathrin-mediated adhesion, and 3) cell endocytosis of NPs that has not yet been explored. These two types of nanosubstrates present the same amount of RGD peptides of varying ligand nanogeometries for studying the dynamic changes of integrin-mediated adhesion and endocytic activity (Figure 1A). We postulate that the AR4-S with a large AR presents a biomimetic hierarchical organization of polypeptides, such as collagen fibrils,[36] to promote cell adhesion behavior but does not favor endocytic uptake of NPs (Figure 1Bii). In contrast, we hypothesize that AR1-S disables the possibility of lateral clustering of integrins for FA maturation[35] but permits the development of endocytic activity (Figure 1Bi). In our findings, we demonstrated that hMSCs cultured on AR1-S showed the enhanced expression of clathrin and AP2 for the formation of clathrin-coated vesicles that facilitate the cellular uptake of NPs. Conversely, AR4-S activated β3 integrin and recruited FA proteins with promoted mechanotransduced signalings, extracellular signal-regulated kinase (ERK), and yes-associated protein (YAP) in hMSCs but much less endocytic uptake of NPs compared to that of AR1-S. We visualized that clathrin and AP2 spatially colocalized with FA in AR4-S group with the formation of clathrin-coated plaques. Mechanistically, pharmacological inhibition of clathrin suppressed cellular uptake of NPs in both groups and substantially reduced nuclear localization of ERK in AR4-S. Meanwhile, the blocking of β3 integrin and the associated FA further boosted the level of NP uptake in both groups. More importantly, utilizing the promoted endocytosis capability of hMSCs on AR1-S by delivering Dex-loaded NPs induced a more robust osteogenic differentiation than those on AR4-S. This work reveals how these engineered nanosubstrates regulate the cellular uptake of suspended drug-loaded

NPs. Moreover, our results not only highlight the altered roles of integrin/clathrin structures in response to nanogeometries of ligand display but also aid the nanosubstrate and nanomedicine development to achieve desired hMSC differentiation for modulating tissue-regenerative processes.

To construct AR1-S and AR4-S, we first synthesized citrate-capped nanospheres (AR1) with a diameter of 36.51 ± 3.85 nm[37] and cetyltrimethylammonium bromide (CTAB)-capped nanorods (AR4) with a length of 77.12 ± 8.67 nm, a width of 18.08 ± 2.13 nm, and an AR of 4.27 ± 0.30,[38] respectively, (Figure 1C,D). Overall, both AR1 and AR4 possessed a similar surface area (~ 4000 nm^2; Figure 1F). The surface plasmon resonance (SPR) peaks of AR1 and AR4 were 530 nm and 866 nm, respectively (Figure 1E). Before nanosubstrate fabrication, we replaced CTAB surfactant of AR4 with citrate by ligand exchange (Figure S1).[39,40] This successful modification was confirmed by ultraviolet-visible absorption spectroscopy that showed similar SPR peaks (Figure S1B) and consecutive changes of zeta potentials throughout the exchange (Figure S1C). Next, we engineered the nanosubstrate by employing mercaptopropylsilatrane (MPS) for thiolation, followed by immobilizing AR1 or AR4 onto the thiolated substrate via Au-thiol linkages, forming AR1-S or AR4-S, respectively (Figure 1A). By optimizing the concentration and incubation time of the NP immobilization, the coating densities of AR1 and AR4 on the substrates were controlled comparable at 41.83 ± 1.24 and 44.55 ± 3.27 NPs/μm^2, respectively (Figure 1G). We verified that high coating density (e.g., exceeding 100 NPs/μm^2) of AR1 or AR4 would cancel out the local anisotropic effect to promote integrin-mediated adhesion (Figure S2). Furthermore, cyclic RGD peptides were conjugated onto the surface of AR1 and AR4 via Au-thiol reaction, resulting in a ligand density of 5691 ± 46 or 5558 ± 141 peptides/NP, respectively (Figure 1G), as quantified by Ellman's assay.[41] Subsequently, the remaining space on the substrate was blocked with maleimide-

terminated polyethylene glycol (PEG) strands via a thiol–maleimide Michael addition click reaction to prevent nonspecific cell adhesion.[35] Our previous studies proved that the covalent bonds (Au-thiol) between AR1 (or AR4) and the thiolated substrate were highly stable to avoid NP internalization by the cells seeded atop or detachment from the substrate throughout the cell culture.[8, 35] Hence, we have fabricated nanosubstrates that present integrin-binding ligands of two distinguished nanogeometries, respectively.

Next, we examined the effect of diverse nanoscale displays of ligands on the endocytosis of drug-loaded NPs in hMSCs. We confirmed that the hMSCs cultured on AR1-S or AR4-S were highly viable (> 90%) over 10 days (Figure S3). Thereafter, we employed graphene quantum dots (GQDs), a well-studied biocompatible zero-dimension NP with a large surface area for drug loading and high fluorescence quantum yield properties for its intracellular tracking.[42,43] GQDs were loaded with Dex (GQD/Dex) to examine the endocytosis capability of hMSCs seeded on AR1-S or AR4-S (Figure 2A). The GQDs purchased from the company emitted a strong fluorescence signal at 450 nm under the excitation of 380 nm (Figure S4). Loading of Dex minimally affected the fluorescence spectrum of GQDs but exhibited the adsorption peak at 242 nm of Dex (Figure S5).[44] The slightly increased physical size of GQD/Dex (3.87 ± 1.04 nm) compared to that of unmodified GQD (1.96 ± 0.36 nm) also indicated the successful loading of Dex to GQDs via π–π stacking (Figure S4 and S5).[45] We verified that GQD/Dex was biocompatible with hMSCs and did not significantly reduce the viability of hMSCs upon incubation of 6 h (Figure S6). Before the uptake, we inserted AR1-S or AR4-S into a tissue culture plate (TCP) well and seeded the cells on top for 24 h. The fluorescence images showed that hMSCs cultured on AR1-S endocytosed more GQD/Dex than those cultured on AR4-S, evidenced by 1-fold higher cytoplasmic fluorescence signals (Figure 2B,C). As literature precedents reported that

GQDs entered the cells through the CME pathway,[46,47] we inhibited clathrin using chlorpromazine, a drug that can hinder the formation of clathrin-coated pits with the adapter proteins from the plasma membrane to intracellular vesicles and also suppress the expression of clathrin.[8,48,49] This inhibition showed a profound decrease of clathrin expression and the intracellular GQD fluorescence signal and minimal effects on the cell viability (Figure 2B,C; Figure S7 and S8). These results demonstrate that AR1-S enhanced the cellular uptake of GQD/Dex by hMSCs via CME pathway.

We investigated whether nanogeometry of ligands regulates adhesion/endocytosis via integrin, as RGD is highly specific to integrin.[50,51] In nanoscale, our Au-immunolabeling results confirmed that integrin β3 engaged with both AR1 and AR4 on the substrates (Figure S9). In microscale, cells showed a higher spreading area with a polygonal shape, more intense stress fibers (F-actin), and larger FA (vinculin) size on AR4-S than those on AR1-S that showed a spindle shape (Figure 2D; Figure S10 and S11). These results suggest that the anisotropic display of ligands by AR4-S enables effective integrin activation for adhesion structure maturation.[35] As previous studies generally demonstrate the conflict between cell adhesion and endocytosis activity,[16] we evaluated the expressions of clathrin and AP2 proteins in cells and their relationship with the adhesion structures in different conditions. Critically, cells expressed an intense dotted pattern of clathrin and AP2 on AR1-S, while these two proteins assembled as FA-like plaques on AR4-S (Figure 2D and Figure S12). Strikingly, more clathrin-coated vesicles on the cytosolic side of plasma membrane were formed in cells on AR1-S, but plaque-like structures with little vesicles were observed in cells on AR4-S, as indicated by Au-immunolabeling (Figure 2E and Figure S13). In addition, cells in AR1-S group expressed higher protein levels of clathrin and AP2 than those in AR4-S group (Figure 2F). These data indicate that hMSCs show endocytosis-active state on AR1-

S and adhesion-active state on AR4-S. Although cells primarily interacted with the AR1 that were immobilized on the substrate surface through the basal membrane, the overall expression of clathrin and AP2 were upregulated in the cells (Figure 2D,F and Figure S12). Meanwhile, our pharmacological blockade of clathrin heavy chain markedly downregulated the expression of clathrin (Figure S8) and reduced the amount of endocytosed GQD/Dex (Figure 2B,C). We conclude that ARS-1 enhances the endocytic activity of the entire cells that were seeded atop, not restricted to the basal membrane area that interacts with the substrate nanostructures.

As cells seeded on AR4-S depicted FA-like clathrin/AP2 plaques, we question their association with adhesion structures. By analyzing Mander's overlap coefficient based on the immunofluorescence staining results, clathrin and AP2 in AR4-S showed significantly higher co-localization/alignment with the F-actin bundles than those in AR1-S (Figure 2D,G and Figure S14). Similar to F-actin, FA showed higher co-localization with AP2 in AR4-S group than AR1-S group (Figure 3A,B). In contrast, integrin β3 highly co-localized with AP2 in both AR1-S and AR4-S groups (Figure S15). These data imply that the integrin β3 in cells that were cultured on AR4-S may be associated with FA/clathrin structures for stabilizing cell adhesion that hinders endocytic activity. Therefore, we suggest that the clathrin may participate in integrin-mediated mechanotransduced signalings in cells on AR4-S (anisotropic ligand presentation), while AR1-S (isotropic ligand presentation) does not support the maturation of FA and promotes CME function. To support this argument, we included two control groups, AR1-S without PEG blocking (Non-blocking AR1-S) and TCP as a blank control, which both provided a homogeneous presentation of cell adhesive peptides on the surface and should empower a well-developed integrin-mediated adhesion.[35,52] As a result, both groups promoted cell spreading and development of FA compared to AR1-S group (Figure S16). In contrast, the immunofluorescence intensity level of AP2 and

relative amounts of endocytosed GQD/Dex in cells decreased in the following order: AR1-S, Non-blocking AR1-S, and TCP (Figure S16 and S17). Thus, the homogeneous display of RGD diminishes the confined nanogeometry effect of AR1-S on enhancing CME activity.

Integrin β3 is one of the cellular receptors to sense the surrounding microenvironment,[53] necessary for cell adhesion and spreading on the RGD-presenting nanosubstrates.[54] The cells in both AR1-S and AR4-S groups adopted integrin β3 to interact with the immobilized RGD on the AuNRs (Figure S9). The inhibition of integrin β3 weakened cell adhesion behaviors in both groups, as evidenced by the decreased cell spreading areas (Figure S18). More importantly, blocking integrin β3 caused a 12% and 97% increase in endocytosed GQD/Dex signals in cells seeded on AR1-S and AR4-S when compared to their untreated counterparts, respectively (Figure 3C,D). This inhibition remarkably reversed this adhesion/endocytosis trend in AR4-S group by suppressing the integrin-mediated mechanosensing signaling that "relinquishes" the clathrin for more endocytic activity. Moreover, this blocking was also effective for the AR1-S group that showed a slight but statically significant (** $P < 0.01$) enhancement of GQD/Dex uptake (Figure 3D), suggesting a further suppression of the integrin β3-mediated mechanotransduction in AR1-S. This result indicates that integrin β3 is a mediator that participates in cell adhesion, and the suppression of FA development rescues CME activity from the strong association with adhesion structures. To further understand this pathway, we employed Y-27632, an inhibitor of Rho-associated protein kinase (ROCK), to suppress cell contractility and focal adhesion.[55] Critically, this pharmacological experiment remarkably promoted the uptake of GQD/Dex (> 1 fold) by cells on AR4-S while slightly increasing the amount of endocytosed GQD/Dex (~ 0.5 fold) by cells on AR1-S (Figure S19), further revealing a potential competitive relationship between cell adhesion and endocytosis. To test the generality of our platform, we have added two more aspect ratio

groups (AR2 and AR7) by constructing AR2-S and AR7-S (Figure S20), and studied the adhesion- (Figure S21) and endocytosis-related behaviors (Figure S22 and S23) of cells that were seeded atop. As expected, considering from AR1-S to AR7-S, the cells cultured on a substrate with AuNRs of large AR (≥ 4) displayed more mature cell adhesion behaviors (e.g., larger spreading area and focal adhesion size) but suppressed cell endocytosis behaviors (e.g., lower expressions of clathrin and AP2 as well as the endocytosed amount of GQD/Dex). In short, we validate the essential roles of nanoscale ligand anisotropy in regulating integrin-associated cell adhesion and endocytosis.

We previously showed that the enhanced cytoskeletal tension via mature FA activated the signaling of mechanosensitive transcriptional factor YAP, which potentiated osteogenic differentiation of hMSCs.[56] Hence, we analyzed the nuclear localization ratio of YAP in the cells primed by AR1-S and AR4-S. Our immunostaining results showed that the cells cultured on AR4-S displayed 43% higher nuclear localization ratio of YAP than those cultured on the AR1-S (Figure S24), confirming the elevated mechanosensing engagement between cells and AR4-S. Furthermore, integrin-mediated mechanotransduced signaling involves the activation of ERK, which can upregulate the transcription activity of runt-related transcription factor 2 (RUNX2), an osteogenic marker of stem cells at early stage.[57] Consistently, the ERK nuclear/cytoplasmic fluorescence intensity ratio in AR4-S group was ~ 2-fold higher than that in AR1-S group (Figure 4), demonstrating the activation of diverse mechanosensing-dependent signalings. Intriguingly, clathrin also participates in modulating this integrin-mediated downstream ERK signaling pathway.[17] Given the high spatial correlation between clathrin/AP2 and FA in cells cultured on AR4-S (Figure 2G and Figure 3A,B), we pharmaceutically inhibited clathrin signaling to study their relationship. Strikingly, this inhibition substantially downregulated the nuclear presence of ERK by 243% in AR4-S group (Figure 4), due to the impediment to integrin/clathrin-mediated

cell adhesion behavior. In contrast, cells cultured on AR1-S already showed 233% lower ERK activity than those on AR4-S, attributed to enhanced endocytosis activity mediated by clathrin. Inhibition of clathrin only slightly decreased the ERK activity by 9% in cells cultured on AR1-S (Figure 4), owing to the original weak role of clathrin in cell adhesion. These findings confirm that the anisotropic display of RGD peptides underpins the engagement between clathrin and adhesion structures for mechanotransduced signalings but refrains from endocytosis.

As there is an imbalanced biophysical environment between AR1-S and AR4-S that respectively influence differentiation potentials of hMSC cultured atop, we wonder whether leveraging the merit of endocytosis-enhancing in AR1-S can alter its differentiation outcome. Hence, we designed two conditions for assessing the enhanced endocytic effect on osteogenic differentiation of hMSCs by AR1-S: (1) cells cultured on the nanosubstrate under osteogenic induction medium with free Dex molecules over 7 days; (2) cells incubated with Dex-delivering nanocarrier, GQD/Dex, on the nanosubstrate under osteogenic induction medium without free Dex molecules (Figure 5A and Figure S25A). Note that the amount of loaded Dex by GQDs in condition (2) was equivalent to that of free Dex in condition (1). Also, cells were preseeded on the nanosubstrate for 24 h before any NP incubation or induced osteogenic differentiation. Besides, we also controlled the duration of GQD/Dex incubation with hMSCs for 6 h, consistent with the cellular uptake experiment (Figure 2B,C). As exocytosis may affect the retention of GQD/Dex inside the cells, we first inspected the fluorescence signals of GQDs inside cells during the 7-day osteogenic differentiation after the 6-h uptake. Interestingly, AR1-S group outperformed AR4-S group in both efficiency of cellular uptake and the retention of NPs (Figure S26). In particular, GQD signals were still detectable in AR1-S group 7 days post cellular uptake but not in AR4-S group (Figure S26), indicating the privilege of AR1-S for acquiring Dex from GQDs. It is known that the acidic

environment in organelle compartments post endocytosis, such as endosome and lysosome,[58] can elicit drug release via weakening the π-π stacking between drugs and GQDs.[59] We also demonstrated that the condition of pH 5 induced a robust cumulative Dex release from GQD/Dex (more than 50% within 1 day) and reached the maxima within 2 days compared to those in pH 7.4 with less than 20 % cumulative Dex release over 7 days (Figure S27), confirming its release mechanism triggered by the intracellular microenvironment.

We assessed the activity of the early stage markers of hMSC osteogenesis, RUNX2 and alkaline phosphatase (ALP) in cells treated with various conditions after 7 days of the differentiation assay.[60,61] As expected, AR4-S group showed a higher nuclear ratio of RUNX2 by 108% (Figure 5B,C) and a higher expression of ALP by 143% (Figure 5D,E and Figure S28) than those in AR1-S group in condition (1), respectively. Strikingly, the relative expression levels of these two markers were significantly enhanced AR1-S group in condition (2), reaching similar levels to those in AR4-S group (Figure 5B–E, S28). Meanwhile, adding GQD alone did not influence these differentiation outcomes (Figure 5B–E). These results are highly consistent with the promoted GQD/Dex uptake via CME in AR1-S group and support the advantage of AR1-S for boosting stem cell osteogenesis. To achieve a synergistic effect of both AR1-S and AR4-S, we cultured the cells on AR1-S first for the uptake of GQD/Dex and next transferred the cells to AR4-S for osteogenic differentiation over 7 days (Figure S25A). Cells primed by this condition expressed a higher level of ALP and more intense nuclear localization of RUNX2 than those cultured on AR1-S or AR4-S only (Figure S25B–E). Hence, cells benefited from both initially enhanced cellular uptake of drug-loaded NPs and subsequently promoted mechanical feedback toward osteogenesis. Nevertheless, this method requires cell harvesting and may disturb the continuity of cell culture, which complicates the process of osteogenesis.

We question whether a second dose of GQD/Dex can further amplify the effect of drug-induced osteogenesis. Hence, we selected Day 4 for the second administration of GQD/Dex and assessed the result on Day 8. We showed that adding Dex molecules and GQD/Dex (1 or 2 doses) to the cells insignificantly affected their viability (Figure S29). Remarkably, AR1-S group even showed ~ 22% more nuclear translocation of RUNX2 and ~ 15% higher percentage of ALP-expressing cells than that of AR4-S group under the 2-dose treatment. We lastly verified that the nanogeometry of ligand presentation (AR1-S or AR4-S) and the GQD/Dex independently affected osteogenic differentiation of the stem cells, evidenced by the lower biomechanical feedback of cells in AR1-S group than those in AR4-S group even after the treatment of GQD/Dex over 7 days of differentiation (Figure S30). This probably stems from blocking the empty space of our platforms with PEG that prevents nonspecific attachment of proteins,[62] decoupling the effect of nanogeometry of ligand presentation on stem cell adhesion from other confounding factors such as adhesion proteins in culture medium or secreted by cells. Hence, we confirm that Dex is critical for the osteogenic differentiation of hMSCs, and hMSCs cultured on AR1-S can benefit from the enhanced drug delivery for intensifying osteogenic differentiation outcomes over the enhanced mechanotransduction on AR4-S.

In conclusion, we elucidated the roles of clathrin in hMSCs for mediating endocytosis or participating in integrin-mediated mechanotransduction by nanosubstrate engineering. Our study modulates the anisotropy of ligand presentation on nanoscale by Au nanostructures with various ARs (1 or 4) and strictly controlled surface areas, particle coating densities, and ligand densities. The cells cultured on AR4-S display higher levels of mechanical feedback in terms of cell adhesion, spreading, and osteogenesis. In contrast, cells on AR1-S show a reverse trend of adhesion-associated events but an elevated expression of clathrin and AP2 that facilitate the uptake of drug-

loaded nanomaterials via CME pathway. Furthermore, we demonstrate that endocytosis may be retarded by a strong association with adhesion structures on AR4-S, as evidenced by the high colocalization between clathrin/AP2 and FA complexes/F-actin and the impeded mechanotransduced signaling ERK pathway by inhibiting clathrin. We manipulate the feature of ligand nanogeometry on AR1-S to maximize osteogenic differentiation outcome by the enhanced uptake of GQD/Dex via robust endocytic activity, regardless of their weak mechanical engagement between integrin and ligand. Our findings not only highlight the dual functions of clathrin in CME and integrin-mediated mechanosensing by tuning the anisotropic ligand nanogeometry, but also provide design rules of nanosubstrates for improving hMSC osteogenesis or other types of differentiations (e.g., adipogenesis) for tissue engineering.

ASSOCIATED CONTENT

Supporting Information

The following files are available free of charge on the ACS Publications website. Experimental methods, characterization of ligand exchange of AR4, cell viability under different treatments, characterization of GQD and GQD/Dex, additional fluorescence images, additional western blot data, additional SEM images, quantification of cell spreading area and FA sizes, quantification of clathrin and AP2 fluorescence intensity in cells, scatter plots of colocalization analysis, additional control experiments, the study of retention of NPs in cells, and Dex release profile.

AUTHOR INFORMATION

Corresponding Author

Siu Hong Dexter Wong: shongwong@polyu.edu.hk

Mo Yang: mo.yang@polyu.edu.hk

Author Contributions

B.Y. conceived the idea, performed experiments, analyzed the data, and drafted the paper. Q.Z., J.C., and C.W. contributed to fluorescence imaging data collection. J.Y., Y.H., and C.L. contributed to TEM imaging data collection. S.H.D.W and M.Y. conceived the idea, contributed to scientific advice, resource for this study, editing of the paper, and supervising the whole project. All authors reviewed and approved the paper.

Notes

The authors declare no competing financial interest.

ACKNOWLEDGMENT

This work was supported by the Shenzhen Science and Technology Program-Basic Research Scheme (JCYJ20220531090808020), the Research Grants Council (RGC) of Hong Kong Collaborative Research Grant (C5078-21 EF), the Research Grants Council (RGC) of Hong Kong General Research Grant (PolyU 15217621 and PolyU 15210818), the Guangdong-Hong Kong Technology Cooperation Funding Scheme (GHP/032/20SZ and SGDX20201103095404018), the Hong Kong Polytechnic University Shenzhen Institute Bai Cheng Bai Yuan Fund (I2022A002),

and the Hong Kong Polytechnic University Internal Fund (1-ZVVQ and 1-CD6J). W.S.H.D. would like to acknowledge the start-up funding (1-ZVRY) from the Department of Biomedical Engineering and Start-up Fund for RAPs under the Strategic Hiring Scheme (1-BD8Q), the Hong Kong Polytechnic University (PolyU, University Grant Council), and PolyU Projects of RISports (1-CD5P) for supporting this work. This work was also supported by the University Research Facility in Life Sciences of the Hong Kong Polytechnic University.

REFERENCES

1. Zhang, Y.; Fang, C.; Zhang, S.; Campbell, R. E.; Serpe, M. J. Controlled osteogenic differentiation of human mesenchymal stem cells using dexamethasone-loaded light-responsive microgels. *ACS Appl. Mater. Interfaces* **2021**, *13*, 7051–7059.
2. Wei, M.; Li, S.; Le, W. Nanomaterials modulate stem cell differentiation: biological interaction and underlying mechanisms. *J. Nanobiotechnol.* **2017**, *15*, 75.
3. Yi, C.; Liu, D.; Fong, C. C.; Zhang, J.; Yang, M. Gold nanoparticles promote osteogenic differentiation of mesenchymal stem cells through p38 MAPK pathway. *ACS Nano* **2010**, *4*, 6439–6448.
4. Madamsetty, V. S.; Mohammadinejad, R.; Uzieliene, I.; Nabavi, N.; Dehshahri, A.; García-Couce, J.; Tavakol, S.; Moghassemi, S.; Dadashzadeh, A.; Makvandi, P. Dexamethasone: Insights into pharmacological aspects, therapeutic mechanisms, and delivery systems. *ACS Biomater. Sci. Eng.* **2022**, *8*, 1763–1790.
5. Bae, S. E.; Choi, D. H.; Han, D. K.; Park, K. Effect of temporally controlled release of dexamethasone on in vivo chondrogenic differentiation of mesenchymal stromal cells. *J. Controlled Release* **2010**, *143*, 23–30.
6. Wang, X.; Li, L.; Song, F. Interplay of nanoparticle properties during endocytosis. Crystals **2021**, *11*, 728.
7. Kovtun, O.; Dickson, V. K.; Kelly, B. T.; Owen, D. J.; Briggs, J. A. G. Architecture of the AP2/clathrin coat on the membranes of clathrin-coated vesicles. *Sci. Adv.* **2020**, *6*, eaba8381.
8. Yin, B.; Ho, L. W. C.; Liu, S.; Hong, H.; Tian, X. Y.; Li, H.; Choi, C. H. J. Sub-10 nm substrate roughness promotes the cellular uptake of nanoparticles by upregulating endocytosis-related genes. *Nano Lett.* **2021**, *21*, 1839–1847.
9. Li, X.; Klausen, L. H.; Zhang, W.; Jahed, Z.; Tsai, C. T.; Li, T. L.; Cui, B. Nanoscale surface topography reduces focal adhesions and cell stiffness by enhancing integrin endocytosis. *Nano Lett.* **2021**, *21*, 8518–8526.
10. Pennacchio, F. A.; Caliendo, F.; Iaccarino, G.; Langella, A.; Siciliano, V.; Santoro, F. Three-dimensionally patterned scaffolds modulate the biointerface at the nanoscale. *Nano Lett.* **2019**, *19*, 5118–5123.
11. Zhao, W.; Hanson, L.; Lou, H. Y.; Akamatsu, M.; Chowdary, P. D.; Santoro, F.; Marks, J. R.; Grassart, A.; Drubin, D. G.; Cui, Y.; Cui, B. Nanoscale manipulation of membrane curvature

for probing endocytosis in live cells. *Nat. Nanotechnol.* **2017**, *12*, 750–756.
12. Huang, C.; Butler, P. J.; Tong, S.; Muddana, H. S.; Bao, G.; Zhang, S. Substrate stiffness regulates cellular uptake of nanoparticles. *Nano Lett.* **2013**, *13*, 1611–1615.
13. Lee, A.; Sousa de Almeida, M.; Milinkovic, D.; Septiadi, D.; Taladriz-Blanco, P.; Loussert-Fonta, C.; Balog, S.; Bazzoni, A.; Rothen-Rutishauser, B.; Petri-Fink, A. Substrate stiffness reduces particle uptake by epithelial cells and macrophages in a size-dependent manner through mechanoregulation. *Nanoscale* **2022**, *14*, 15141–15155.
14. Elkhatib, N.; Bresteau, E.; Baschieri, F.; Rioja, A. L.; van Niel, G.; Vassilopoulos, S.; Montagnac, G. Tubular clathrin/AP-2 lattices pinch collagen fibers to support 3D cell migration. *Science* **2017**, *356*, eaal4713.
15. Leyton-Puig, D.; Isogai, T.; Argenzio, E.; van den Broek, B.; Klarenbeek, J.; Janssen, H.; Jalink, K.; Innocenti, M. Flat clathrin lattices are dynamic actin-controlled hubs for clathrin-mediated endocytosis and signalling of specific receptors. *Nat. Commun.* **2017**, *8*, 16068.
16. Yu, C. H.; Rafiq, N. B.; Cao, F.; Zhou, Y.; Krishnasamy, A.; Biswas, K. H.; Ravasio, A.; Chen, Z.; Wang, Y. H.; Kawauchi, K.; Jones, G. E.; Sheetz, M. P. Integrin-beta3 clusters recruit clathrin-mediated endocytic machinery in the absence of traction force. *Nat. Commun.* **2015**, *6*, 8672.
17. Baschieri, F.; Dayot, S.; Elkhatib, N.; Ly, N.; Capmany, A.; Schauer, K.; Betz, T.; Vignjevic, D. M.; Poincloux, R.; Montagnac, G. Frustrated endocytosis controls contractility-independent mechanotransduction at clathrin-coated structures. *Nat. Commun.* **2018**, *9*, 3825.
18. Lock, J. G.; Baschieri, F.; Jones, M. C.; Humphries, J. D.; Montagnac, G.; Stromblad, S.; Humphries, M. J. Clathrin-containing adhesion complexes. *J. Cell Biol.* **2019**, *218*, 2086–2095.
19. Almalik, A.; Karimi, S.; Ouasti, S.; Donno, R.; Wandrey, C.; Day, P. J.; Tirelli, N., Hyaluronic acid (HA) presentation as a tool to modulate and control the receptor-mediated uptake of HA-coated nanoparticles. *Biomaterials* **2013**, *34*, 5369–5380.
20. Zhu, C.; Zhou, X.; Liu, Z.; Chen, H.; Wu, H.; Yang, X.; Zhu, X.; Ma, J.; Dong, H. The morphology of hydroxyapatite nanoparticles regulates cargo recognition in clathrin-mediated endocytosis. *Front. Mol. Biosci.* **2021**, *8*, 627015.
21. Adler, A. F.; Leong, K. W. Emerging links between surface nanotechnology and endocytosis: impact on nonviral gene delivery. *Nano today* **2010**, *5*, 553–569.
22. Teo, B. K.; Goh, S. H.; Kustandi, T. S.; Loh, W. W.; Low, H. Y.; Yim, E. K. The effect of micro and nanotopography on endocytosis in drug and gene delivery systems. *Biomaterials* **2011**, *32*, 9866–9875.
23. Karimi, F.; Thombare, V. J.; Hutton, C. A.; O'Connor, A. J.; Qiao, G. G.; Heath, D. E. Beyond RGD; nanoclusters of syndecan- and integrin-binding ligands synergistically enhance cell/material interactions. *Biomaterials* **2018**, *187*, 81–92.
24. Ye, K.; Wang, X.; Cao, L.; Li, S.; Li, Z.; Yu, L.; Ding, J. Matrix stiffness and nanoscale spatial organization of cell-adhesive ligands direct stem cell fate. *Nano Lett.* **2015**, 15, 4720–4729.
25. Kang, H.; Wong, S. H. D.; Pan, Q.; Li, G.; Bian, L. Anisotropic ligand nanogeometry modulates the adhesion and polarization state of macrophages. *Nano Lett.* **2019**, *19*, 1963–1975.
26. Liu, W.; Sun, Q.; Zheng, Z. L.; Gao, Y. T.; Zhu, G. Y.; Wei, Q.; Xu, J. Z.; Li, Z. M.; Zhao, C. S. Topographic cues guiding cell polarization via distinct cellular mechanosensing pathways. *Small* **2022,** *18*, e2104328.
27. Yao, X.; Peng, R.; Ding, J. Cell-material interactions revealed via material techniques of surface patterning. *Adv. Mater.* **2013**, *25*, 5257–5286.
28. Wang, X.; Yan, C.; Ye, K.; He, Y.; Li, Z.; Ding, J. Effect of RGD nanospacing on

differentiation of stem cells. *Biomaterials* **2013**, *34*, 2865–2874.
29. Wang, X.; Li, S.; Yan, C.; Liu, P.; Ding, J. Fabrication of RGD micro/nanopattern and corresponding study of stem cell differentiation. *Nano Lett.* **2015**, *15*, 1457–1467.
30. Sun, Q.; Pei, F.; Zhang, M.; Zhang, B.; Jin, Y.; Zhao, Z.; Wei, Q. Curved nanofiber network induces cellular bridge formation to promote stem cell mechanotransduction. *Adv. Sci.* **2023**, *10*, e2204479.
31. Yin, B.; Yang, H.; Yang, M. Integrating soft hydrogel with nanostructures reinforces stem cell adhesion and differentiation. *J. Compos. Sci.* **2022**, *6*, 19.
32. Wong, D. S.; Li, J.; Yan, X.; Wang, B.; Li, R.; Zhang, L.; Bian, L. Magnetically tuning tether mobility of integrin ligand regulates adhesion, spreading, and differentiation of stem cells. *Nano Lett.* **2017**, *17*, 1685–1695.
33. Wong, S. H. D.; Wong, W. K. R.; Lai, C. H. N.; Oh, J.; Li, Z.; Chen, X.; Yuan, W.; Bian, L. Soft polymeric matrix as a macroscopic cage for magnetically modulating reversible nanoscale ligand presentation. *Nano Lett.* **2020**, *20*, 3207–3216.
34. Di Natale, C.; Natale, C. F.; Florio, D.; Netti, P. A.; Morelli, G.; Ventre, M.; Marasco, D. Effects of surface nanopatterning on internalization and amyloid aggregation of the fragment 264-277 of Nucleophosmin 1. *Colloids Surf., B* **2021**, *197*, 111439.
35. Wong, S. H. D.; Yin, B.; Yang, B.; Lin, S.; Li, R.; Feng, Q.; Yang, H.; Zhang, L.; Yang, Z.; Li, G. Anisotropic nanoscale presentation of cell adhesion ligand enhances the recruitment of diverse integrins in adhesion structures and mechanosensing-dependent differentiation of stem cells. *Adv. Funct. Mater.* **2019**, *29*, 1806822.
36. Gautieri, A.; Vesentini, S.; Redaelli, A.; Buehler, M. J. Hierarchical structure and nanomechanics of collagen microfibrils from the atomistic scale up. *Nano Lett.* **2011**, *11*, 757–766.
37. Bastus, N. G.; Comenge, J.; Puntes, V. Kinetically controlled seeded growth synthesis of citrate-stabilized gold nanoparticles of up to 200 nm: size focusing versus Ostwald ripening. *Langmuir* **2011**, *27*, 11098–110105.
38. Yang, H.; Chen, Z.; Zhang, L.; Yung, W. Y.; Leung, K. C.; Chan, H. Y.; Choi, C. H. Mechanism for the cellular uptake of targeted gold nanorods of defined aspect ratios. *Small* **2016**, *12*, 5178–5189.
39. Mehtala, J. G.; Zemlyanov, D. Y.; Max, J. P.; Kadasala, N.; Zhao, S.; Wei, A. Citrate-stabilized gold nanorods. *Langmuir* **2014**, *30*, 13727–13730.
40. Oh, J.; Xia, X.; Wong, W. K. R.; Wong, S. H. D.; Yuan, W.; Wang, H.; Lai, C. H. N.; Tian, Y.; Ho, Y. P.; Zhang, H.; Zhang, Y.; Li, G.; Lin, Y.; Bian, L. The effect of the nanoparticle shape on T cell activation. *Small* **2022**, *18*, e2107373.
41. Yin, B.; Chan, C. K. W.; Liu, S.; Hong, H.; Wong, S. H. D.; Lee, L. K. C.; Ho, L. W. C.; Zhang, L.; Leung, K. C.; Choi, P. C.; Bian, L.; Tian, X. Y.; Chan, M. N.; Choi, C. H. J. Intrapulmonary cellular-level distribution of inhaled nanoparticles with defined functional groups and its correlations with protein corona and inflammatory response. *ACS Nano* **2019**, *13*, 14048–14069.
42. Shang, W.; Zhang, X.; Zhang, M.; Fan, Z.; Sun, Y.; Han, M.; Fan, L. The uptake mechanism and biocompatibility of graphene quantum dots with human neural stem cells. *Nanoscale* **2014**, *6*, 5799–5806.
43. Ghaffarkhah, A.; Hosseini, E.; Kamkar, M.; Sehat, A. A.; Dordanihaghighi, S.; Allahbakhsh, A.; van der Kuur, C.; Arjmand, M. Synthesis, applications, and prospects of graphene quantum dots: A comprehensive review. *Small* **2022**, *18*, 2102683.
44. Devi, G. R.; Prathyusha, V.; Shanthakumari, K.; Rahaman, S. Development and validation

of UV-Spectrophotometric method for the estimation of dexamethasone sodium phosphate in bulk and pharmaceutical dosage form. *Indo Am. J. Pharm. Res* **2013**, *3*, 5055–5061.
45. Hao, Y.; Zhang, F.; Mo, S.; Zhao, J.; Wang, X.; Zhao, Y.; Zhang, L. Biomedical applications of supramolecular materials in the controllable delivery of steroids. *Front. Mol. Biosci.* **2021**, *8*, 700712.
46. Das, G.; Benyettou, F.; Sharma, S. K.; Sharama, S. K.; Prakasam, T.; Gandara, F.; de la Pena-O'Shea, V. A.; Saleh, N.; Pasricha, R.; Jagannathan, R.; Olson, M. A.; Trabolsi, A. Covalent organic nanosheets for bioimaging. *Chem. Sci.* **2018**, *9*, 8382–8387.
47. Chen, X.; Fan, Y.; Sun, J.; Zhang, Z.; Xin, Y.; Li, K.; Tang, K.; Du, P.; Liu, Y.; Wang, G.; Yang, M.; Tan, Y. Nanoparticle-mediated specific elimination of soft cancer stem cells by targeting low cell stiffness. *Acta Biomater.* **2021**, *135*, 493–505.
48. Vercauteren, D.; Vandenbroucke, R. E.; Jones, A. T.; Rejman, J.; Demeester, J.; De Smedt, S. C.; Sanders, N. N.; Braeckmans, K., The use of inhibitors to study endocytic pathways of gene carriers: optimization and pitfalls. *Mol. Ther.* **2010,** *18*, 561–569.
49. Zhang, Y.; Zhang, L.; Li, Y.; Sun, S.; Tan, H. Different contributions of clathrin- and caveolae-mediated endocytosis of vascular endothelial cadherin to lipopolysaccharide-induced vascular hyperpermeability. *PLoS One* **2014,** *9*, e106328.
50. Acharya, A. P.; Dolgova, N. V.; Moore, N. M.; Xia, C. Q.; Clare-Salzler, M. J.; Becker, M. L.; Gallant, N. D.; Keselowsky, B. G. The modulation of dendritic cell integrin binding and activation by RGD-peptide density gradient substrates. *Biomaterials* **2010**, *31*, 7444–7454.
51. Wirkner, M.; Weis, S.; San Miguel, V.; Alvarez, M.; Gropeanu, R. A.; Salierno, M.; Sartoris, A.; Unger, R. E.; Kirkpatrick, C. J.; del Campo, A. Photoactivatable caged cyclic RGD peptide for triggering integrin binding and cell adhesion to surfaces. *Chembiochem* **2011**, *12*, 2623–2629.
52. Hou, Y.; Yu, L.; Xie, W.; Camacho, L. C.; Zhang, M.; Chu, Z.; Wei, Q.; Haag, R. Surface roughness and substrate stiffness synergize to drive cellular mechanoresponse. *Nano Lett.* **2020**, *20*, 748–757.
53. Xie, W.; Wei, X.; Kang, H.; Jiang, H.; Chu, Z.; Lin, Y.; Hou, Y.; Wei, Q. Static and dynamic: Evolving biomaterial mechanical properties to control cellular mechanotransduction. *Adv. Sci.* **2023,** *10*, e2204594.
54. Jeschke, B.; Meyer, J.; Jonczyk, A.; Kessler, H.; Adamietz, P.; Meenen, N. M.; Kantlehner, M.; Goepfert, C.; Nies, B. RGD-peptides for tissue engineering of articular cartilage. *Biomaterials* **2002**, *23*, 3455–3463.
55. Yang, B.; Wei, K.; Loebel, C.; Zhang, K.; Feng, Q.; Li, R.; Wong, S. H. D.; Xu, X.; Lau, C.; Chen, X.; Zhao, P.; Yin, C.; Burdick, J. A.; Wang, Y.; Bian, L. Enhanced mechanosensing of cells in synthetic 3D matrix with controlled biophysical dynamics. *Nat. Commun.* **2021,** *12*, 3514.
56. Zhang, C.; Zhu, H.; Ren, X.; Gao, B.; Cheng, B.; Liu, S.; Sha, B.; Li, Z.; Zhang, Z.; Lv, Y.; Wang, H.; Guo, H.; Lu, T. J.; Xu, F.; Genin, G. M.; Lin, M. Mechanics-driven nuclear localization of YAP can be reversed by N-cadherin ligation in mesenchymal stem cells. *Nat. Commun.* **2021**, *12*, 6229.
57. Eskildsen, T.; Taipaleenmäki, H.; Stenvang, J.; Abdallah, B. M.; Ditzel, N.; Nossent, A. Y.; Bak, M.; Kauppinen, S.; Kassem, M. MicroRNA-138 regulates osteogenic differentiation of human stromal (mesenchymal) stem cells in vivo. *Proc. Natl. Acad. Sci., U. S. A.* **2011**, *108*, 6139–6144.
58. Hu, Y. B.; Dammer, E. B.; Ren, R. J.; Wang, G. The endosomal-lysosomal system: from acidification and cargo sorting to neurodegeneration. *Transl. Neurodegener.* **2015**, *4*, 18.
59. Zhuang, W. R.; Wang, Y.; Cui, P. F.; Xing, L.; Lee, J.; Kim, D.; Jiang, H. L.; Oh, Y. K.

Applications of pi-pi stacking interactions in the design of drug-delivery systems. *J. Controlled Release* **2019**, *294*, 311–326.
60. Lee, K.-S.; Kim, H.-J.; Li, Q.-L.; Chi, X.-Z.; Ueta, C.; Komori, T.; Wozney, J. M.; Kim, E.-G.; Choi, J.-Y.; Ryoo, H.-M. Runx2 is a common target of transforming growth factor β1 and bone morphogenetic protein 2, and cooperation between Runx2 and Smad5 induces osteoblast-specific gene expression in the pluripotent mesenchymal precursor cell line C2C12. *Mol. Cell. Biol.* **2000**, *20*, 8783–8792.
61. Li, N.; Zhou, L.; Xie, W.; Zeng, D.; Cai, D.; Wang, H.; Zhou, C.; Wang, J.; Li, L. Alkaline phosphatase enzyme-induced biomineralization of chitosan scaffolds with enhanced osteogenesis for bone tissue engineering. *Chem. Eng. J.* **2019**, *371*, 618–630.
62. Du, H.; Chandaroy, P.; Hui, S. W. Grafted poly-(ethylene glycol) on lipid surfaces inhibits protein adsorption and cell adhesion. *Biochim. Biophys. Acta* **1997,** *1326*, 236–248.

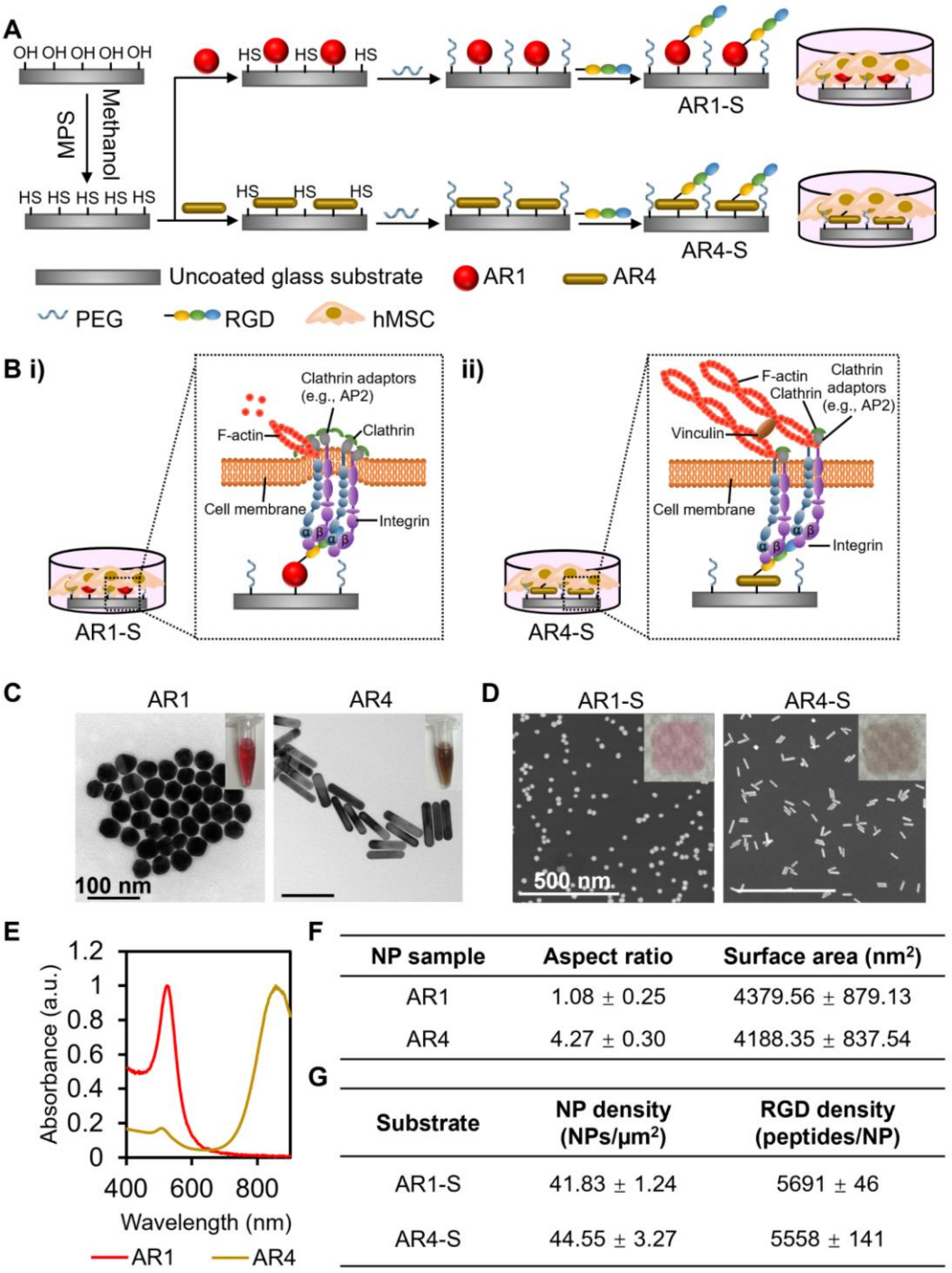

F

NP sample	Aspect ratio	Surface area (nm²)
AR1	1.08 ± 0.25	4379.56 ± 879.13
AR4	4.27 ± 0.30	4188.35 ± 837.54

G

Substrate	NP density (NPs/μm²)	RGD density (peptides/NP)
AR1-S	41.83 ± 1.24	5691 ± 46
AR4-S	44.55 ± 3.27	5558 ± 141

Figure 1. Characterization of glass substrates with ligand nanogeometry created by gold nanorods (AuNRs). (A) Schematic illustration of surface modification of a glass substrate with AuNRs with an aspect ratio (AR) of 1 or 4 (denoted AR1 or AR4) to form AR1-S or AR4-S, respectively. AR1-S and AR4-S refer to the insertion of an AR1 or AR4-coated glass substrate to a well of a conventional 24-well tissue culture plate (TCP), respectively. (B) Schematic postulation of how (i) AR1-S and (ii) AR4-S regulate cell endocytosis and adhesion structures. (C) Representative transmission electron microscopy (TEM) images reveal the morphology of AR1 and AR4

suspended in nanopure water. (D) Scanning electron microscopy (SEM) images reveal the morphology and coating density of AR1-S and AR4-S. (E) ultra-violet–visible (UV–vis) spectra of AR1 and AR4 suspended in nanopure water with surface plasmon resonance (SPR) peaks at 530 nm and 866 nm, respectively. (F) Quantification of AR and surface area of AR1 and AR4 by counting at least 50 nanoparticles (NPs) in TEM images. (G) Quantification of NP density and Arg-Gly-Asp (RGD) density by analyzing at least 10 SEM images of 1 μm × 1μm. Error bar denotes the standard deviation resulting from three independent experiments.

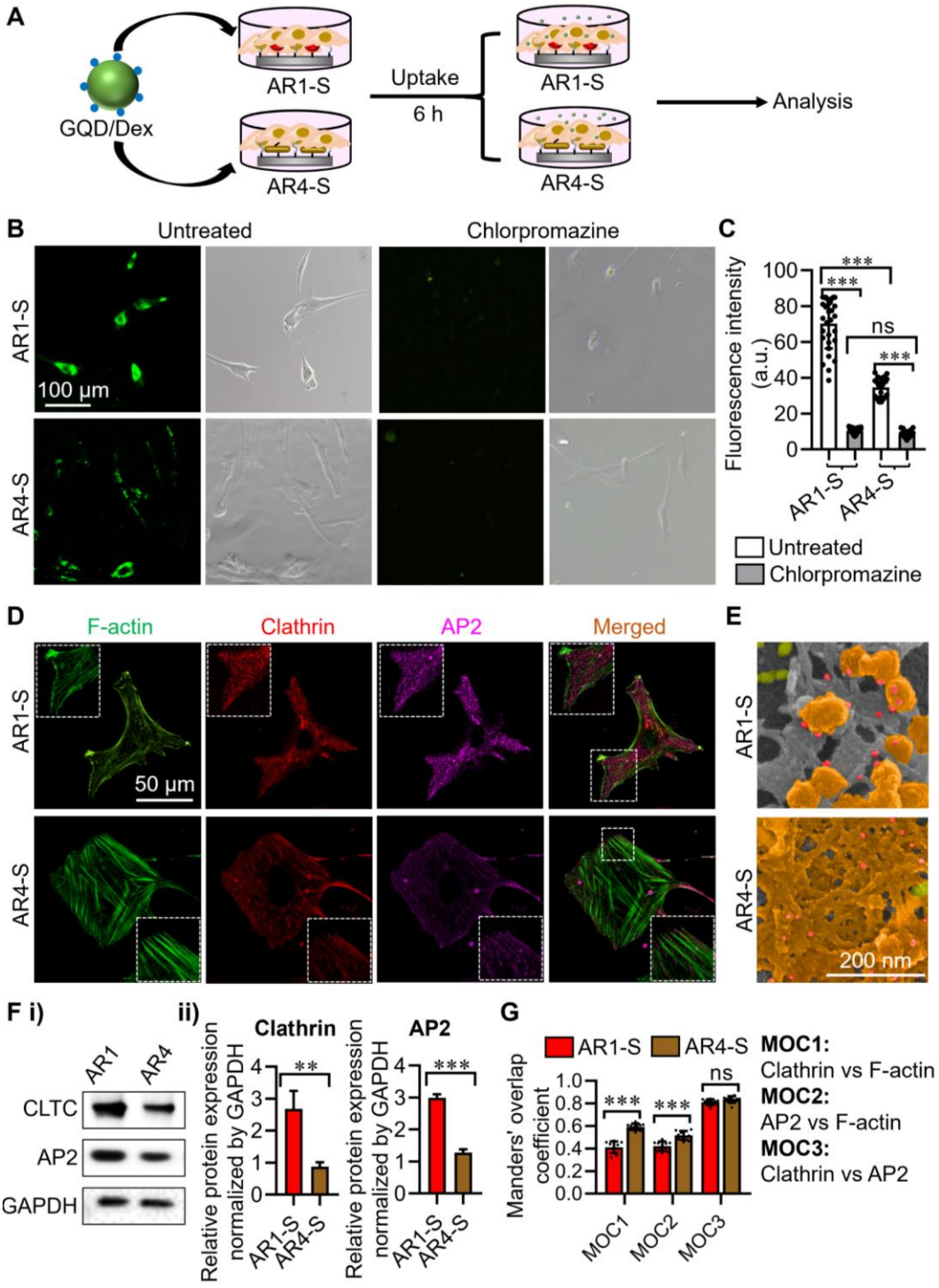

Figure 2. Examination of endocytic activity and uptake of dexamethasone (Dex)-loaded graphene quantum dots (GQDs; GQD/Dex) by hMSCs that were seeded on AR1-S or AR4-S. (A) Schematic illustration of cellular uptake experiment. The cells were preseeded on the AR1-S or AR4-S in a culture well and incubated with a growth medium for 24 h. During cellular uptake, the cells were incubated with GQD/Dex for 6 h. The relative amount of GQD/Dex internalized by cells was measured by fluorescence microscopy. (B) Representative fluorescence and optical images of

hMSCs after endocytosis of GQD/Dex with or without pretreatment of 5 μg/mL chlorpromazine (inhibitor of clathrin) in both AR1-S and AR4-S groups. (C) Quantitative analysis of fluorescence signals in cells from different groups corresponding to (B). Averaged fluorescence signals of GQD/Dex were measured in each cell. 20 cells were examined for each group. (D) Representative fluorescence images of cells that were seeded on AR1-S or AR4-S for 24 h, followed by immunostaining of the filamentous actin (F-actin, green), clathrin (red), and adaptor protein 2 (AP2, purple). (E) Representative SEM images show 13 nm AuNPs preadsorbed with goat anti-mouse (H+L) IgG, binding to cells that were cultured on the substrates after 24 h and further preincubated with mouse anti-human clathrin overnight. Clathrin, 13 nm AuNP, and the NP on the substrates (AR1 and AR4) were painted with the pseudocolors orange, red, and golden yellow, respectively. (F) Western blotting results of clathrin heavy chain (CLTC) and AP2 in cells seeded on AR1-S and AR4-S with ii) statistical analysis. (G) Quantitative analysis of co-localization measured between clathrin/AP2 and F-actin by MOC with Costes (≥ 95%) involving at least 10 cells. Statistical analysis of pairwise comparison was determined by one-way ANOVA. No significance (ns): $P > 0.05$; ** $P < 0.01$; *** $P < 0.001$.

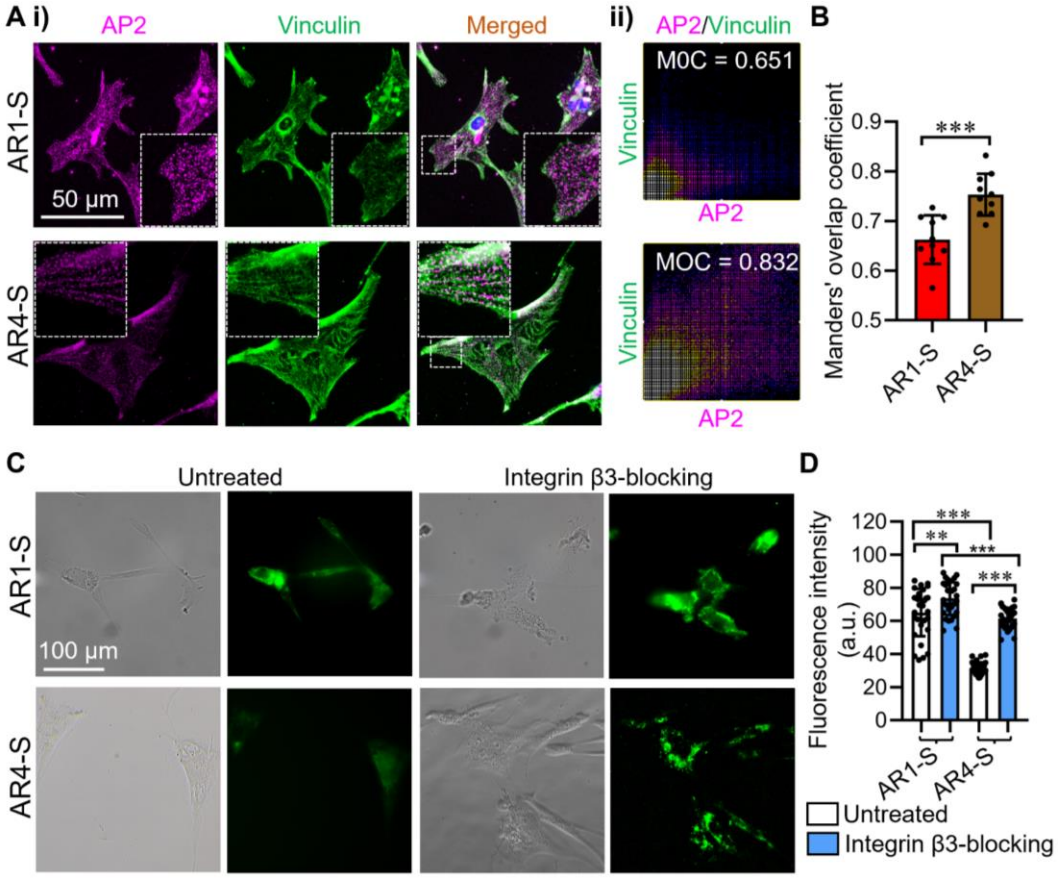

Figure 3. Evaluation of clathrin and AP2 in the role of endocytosis and integrin-mediated mechanosensing. (A) (i) Representative fluorescence images of cells that were seeded on AR1-S or AR4-S for 24 h, followed by immunostaining against AP2 (purple) and vinculin (green). (ii)

Quantitative colocalization of AP2 and vinculin scatter plots of the boxed areas as shown in (i). The numbers indicate the MOC. (B) Quantitative analysis of co-localization measured by MOC with Costes (≥ 95%) involving 10 cells cultured on AR1-S or AR4-S. (C) Representative fluorescence images of hMSCs after endocytosis of GQD/Dex with or without pretreatment of 5 μg/mL integrin β3 in both AR1-S and AR4-S groups. (D) Quantitative analysis of fluorescence signals in cells from different groups corresponding to (C). Averaged fluorescence signals of GQD/Dex were measured in each cell. 20 cells were examined for each group. Statistical analysis of pairwise comparison was determined by one-way ANOVA. ** $P < 0.01$; *** $P < 0.001$.

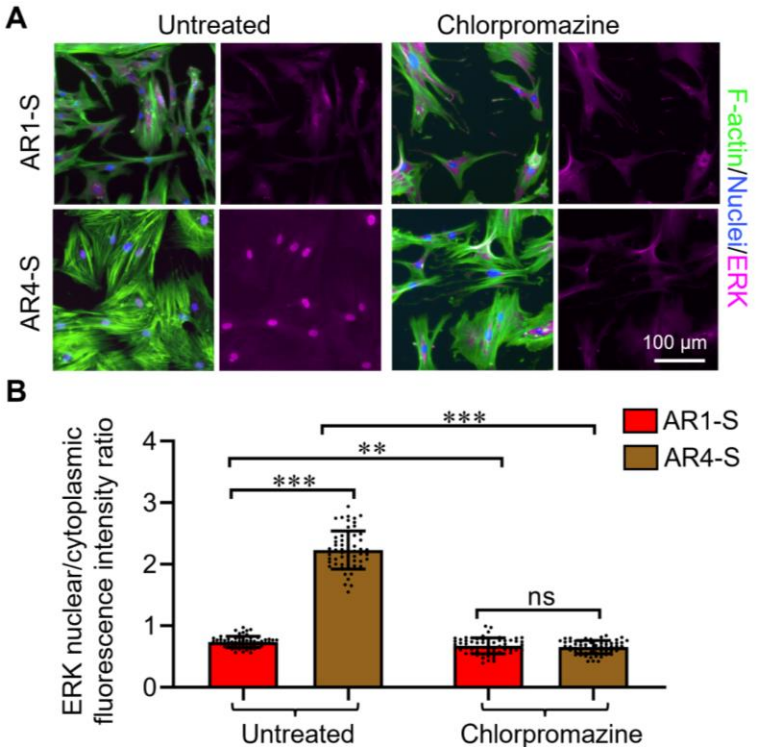

Figure 4. Evaluation of clathrin in the role of promoting mechanotransduction-based signaling. (A) Representative fluorescence images of cells that were seeded on AR1-S or AR4-S for 24 h, followed by immunostaining of the F-actin (green), nucleus (blue), and signal-regulated kinase (ERK) with or without pretreatment of 5 μg/mL chlorpromazine. (B) Quantitative analysis of fluorescence signals in cells from different groups corresponding to (A). 30 cells were examined for each group. Statistical analysis of pairwise comparison was determined by one-way ANOVA. No significance (ns): $P > 0.05$; ** $P < 0.01$; *** $P < 0.001$.

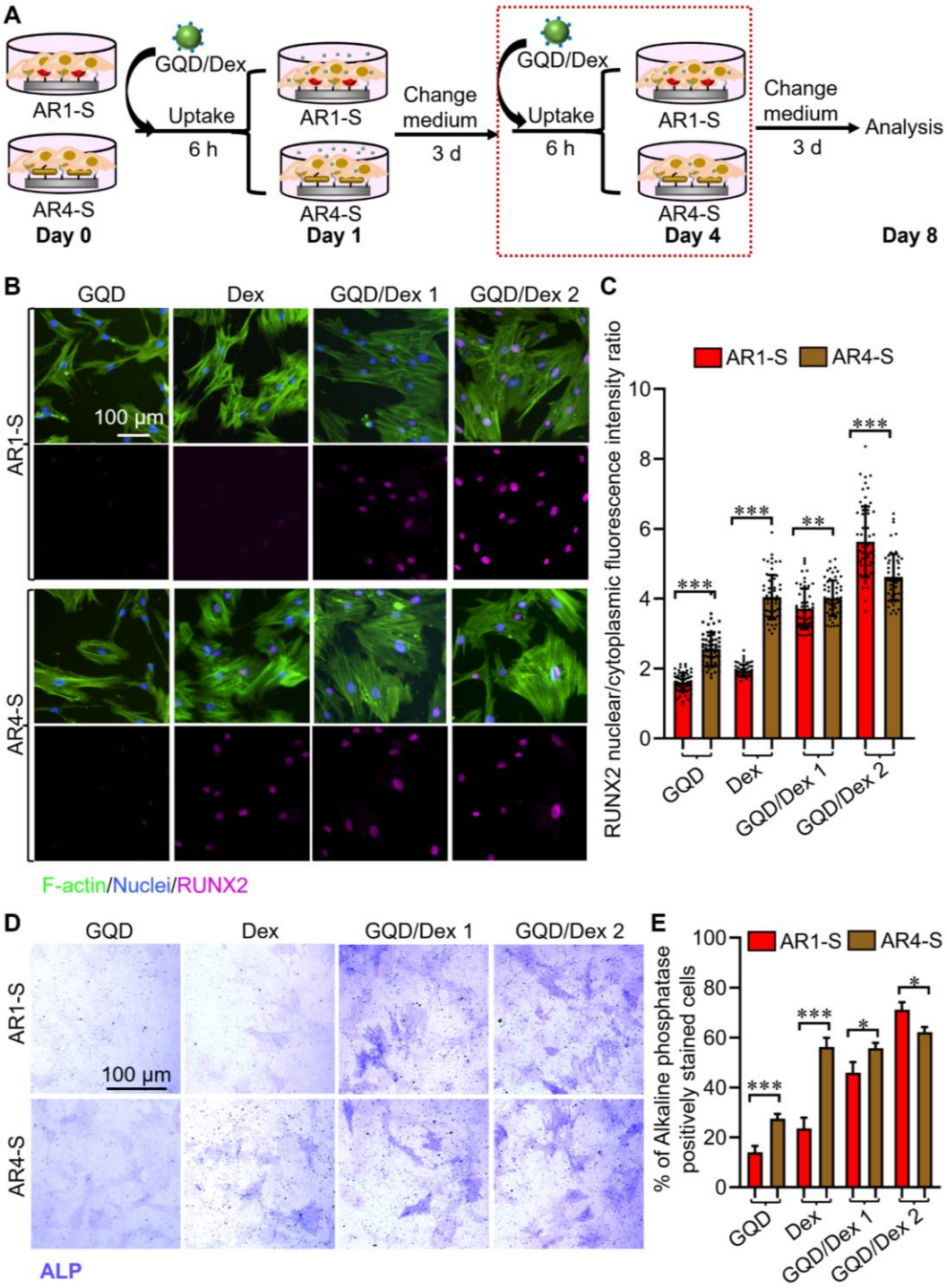

Figure 5. Osteogenesis differentiation of hMSCs induced by GQD/Dex when conditioned to AR1-S and AR4-S, respectively. (A) Schematic illustration of differentiation experiment. The cells were preseeded on the AR1-S or AR4-S in a culture well on Day 0 and incubated with growth medium for 24 h. On Day 1, the cells were incubated with or without GQD/Dex for 6 h, and the particle-containing medium was replaced by osteogenesis induction medium. On Day 4, the cells were or were not incubated with GQD/Dex as the second dose for 6 h, and the particle-containing medium was replaced by osteogenesis medium. The cell osteogenesis was analyzed on Day 8. (B)

Representative fluorescence images of cells after different treatments on Day 8, followed by immunostaining of the F-actin (green), nucleus (blue), and Runt-related transcription factor 2 (RUNX2, purple). (C) Quantitative analysis of fluorescence signals in cells from different groups corresponding to (B). 30 cells were examined for each group. (D) Representative images of cells after different treatments on Day 8, followed by staining of alkaline phosphatase (ALP, purple). (E) Quantitative analysis of the percentage of ALP-positive cells from different groups corresponding to (D). Error bar denotes the standard deviation resulting from three independent experiments. Statistical analysis of pairwise comparison was determined by one-way ANOVA. Significance difference: * $P < 0.05$; ** $P < 0.01$; *** $P < 0.001$.

TABLE OF CONTENT (TOC) GRAPHIC